Design of a Multiband OFDM System for Realistic UWB Channel Environments

Anuj Batra, *Member, IEEE*, Jaiganesh Balakrishnan, *Member, IEEE*, G. Roberto Aiello, *Member, IEEE*,
Jeffrey R. Foerster, *Member, IEEE*, and Anand Dabak, *Member, IEEE*

Invited Paper

Abstract—In February 2002, the Federal Communications Commission allocated 7500 MHz of spectrum for unlicensed use of commercial ultra-wideband (UWB) communication devices. This spectral allocation has initiated an extremely productive activity for industry and academia. Wireless communications experts now consider UWB as available spectrum to be utilized with a variety of techniques, and not specifically related to the generation and detection of short RF pulses as in the past.

There are many differences between real-world behavior of narrow-band and UWB systems. All wireless systems must be able to deal with the challenges of operating over a multipath propagation channel, where objects in the environment can cause multiple reflections to arrive at the receiver (RX). For narrow-band systems, these reflections will not be resolvable by the RX when the narrow-band system bandwidth is less than the coherence bandwidth of the channel. The large bandwidth of UWB waveforms, instead, significantly increases the ability of the RX to resolve the different reflections in the channel. The UWB channel model developed by the IEEE 802.15.3a standard body is described in this paper.

For highly dispersive channels, an orthogonal frequency-division multiplexing (OFDM) RX is more efficient at capturing multipath energy than an equivalent single-carrier system using the same total bandwidth. OFDM systems possess additional desirable properties, such as high spectral efficiency, inherent resilience to narrow-band RF interference, and spectral flexibility, which is important because the regulatory rules for UWB devices have not been finalized throughout the entire world. This paper describes the design of a UWB system optimized for very high bit-rate, low-cost, and low-power wireless networks for personal computing (PC), consumer electronics (CE), and mobile applications. The system combines OFDM modulation technique with a multibanding approach, which divides the spectrum into several sub-bands, whose bandwidth is approximately 500 MHz.

The system described in this paper has been selected by several key industry organizations [Mulitband OFDM Alliance, Wi-Media, Wireless Universal Serial Bus (USB)] because of its very good technical characteristics for the diverse set of high performance short-range applications that are eagerly anticipated for CE, PC, and mobile applications.

Index Terms—Multiband orthogonal frequency-division multiplexing (OFDM), ultra-wideband (UWB), wireless personal area networks (WPANs).

I. INTRODUCTION

WHEN THE Federal Communications Commission (FCC) agreed in February 2002 to allocate 7500 MHz of spectrum for unlicensed use of ultra-wideband (UWB) devices for communication applications in the 3.1–10.6-GHz frequency band [1], the move represented a victory in a long hard-fought battle that dated back decades. With its origins in the 1960s, when it was called time-domain electromagnetics, UWB came to be known for the operation of sending and receiving extremely short bursts of RF energy. With its outstanding ability for applications that require precision distance or positioning measurements, as well as high-speed wireless connectivity, the largest spectrum allocation ever granted by the FCC is unique because it overlaps other services in the same frequency of operation.

Previous spectrum allocations for unlicensed use, such as the Unlicensed National Information Infrastructure (UNII) band, have opened up bandwidth dedicated to unlicensed devices based on the assumption that "operation is subject to the following two conditions: (1) This device may not cause harmful interference, and (2) this device must accept any interference received, including interference that may cause undesired operation."[1] Harmful interference is defined as "[i]nterference that ... seriously degrades, obstructs or repeatedly interrupts a radio communication service."[2] This means that devices using unlicensed spectrum must be designed to coexist in an uncontrolled environment.

Devices utilizing UWB spectrum operate according to similar rules, but they are subject to more stringent requirements because UWB spectrum underlays other existing licensed and unlicensed spectrum allocations. In order to optimize spectrum use and reduce interference to existing services, the FCC's regulations are very conservative and require very low emitted power from UWB devices.

The FCC requires that UWB devices occupy more than 500 MHz of bandwidth in the 3.1–10.6-GHz band, according to

[1]FCC 47 C.F.R. Sec. 15.5(b).
[2]FCC 47 C.F.R., 1.907, Sec. 2.1.

UWB Emission Limit for Outdoor Hand-held Systems
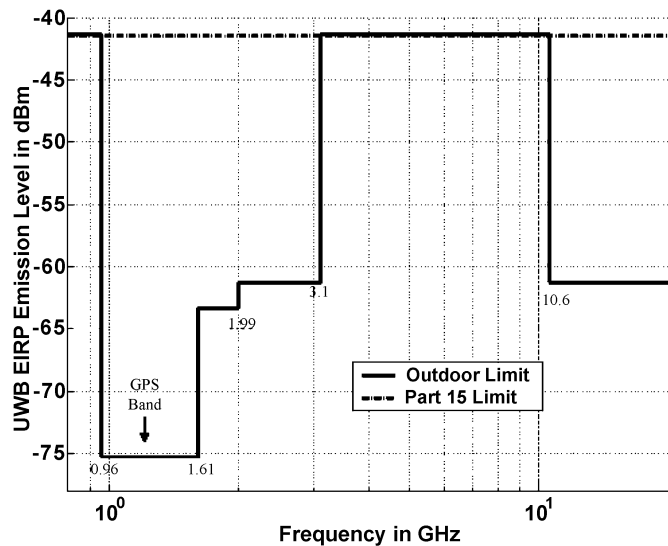

Fig. 1. UWB spectral mask for outdoor communication systems. Emission level is measured in 1-MHz bandwidth.

TABLE I
SUMMARY OF PHY REQUIREMENTS

Parameter	Value
Bit rate (PHY Layer)	110 Mbps
	200 Mbps
	480Mbps
Range	10 m
	4 m
	2 m
Power consumption (PHY Layer)	100mW
	250mW
	No valued specified
Target bit error rate	10^{-5}
Co-located piconets	4

the spectrum mask in Fig. 1. The power spectral density (PSD) measured in 1-MHz bandwidth must not exceed the specified -41.25 dBm, which is low enough not to cause interference to other services operating under different rules, but sharing the same bandwidth. Cellular phones, for example, transmit up to $+30$ dBm, which is equivalent to 10^7 higher PSD than UWB transmitters (TXs) are permitted.

This presents a serious challenge to any UWB system because other services sharing the same band of operation on licensed or unlicensed bands are likely to have a much higher transmit power and, therefore, would subject UWB receivers (RXs) to considerable interference.

This spectral allocation has initiated an extremely productive activity for industry and academia. Wireless communications experts now consider UWB as available spectrum to be utilized with a variety of techniques, and not specifically related to the generation and detection of short RF pulses, as in the past.

One of the most innovative techniques involves utilizing only 500-MHz instantaneous bandwidth (the minimum amount allowed by the FCC ruling) and dividing that frequency band into smaller simultaneously transmitted sub-carriers. Such systems present high regulatory flexibility for worldwide operation because they enable independent control of portions of the emitted spectrum to adapt for different environments.

A design based on this idea is the best technical solution for very high bit-rate, low-cost, and low-power wireless networks for personal computing (PC), consumer electronics (CE), and mobile applications. These applications can be satisfied by relatively short-range systems, within a user's personal space, assuming that all other performance requirements are met.

Systems developed to date, such as IEEE 802.11b, 11a, or 11g, do not address this market because they are designed to integrate longer-range wireless networks and are integrated on devices that can support higher power consumption and cost. A specification is emerging today, led by the multiband orthog-

onal frequency-division multiplexing alliance (MBOA),[3] which is optimized to support these applications. The purpose of this standard is to provide a specification for wireless connectivity among devices within or entering the personal operating space. The data rate must be high enough (greater than 110 Mb/s) to satisfy a set of CE and multimedia industry needs for wireless personal area network (WPAN) communications. The standard also addresses the quality of service (QoS) capabilities required to support multimedia data types and mobile scenarios. There is also an extremely strong interest for even higher throughput and shorter range, up to 480 Mb/s, to support applications such as Wireless Universal Serial Buse (USB) or Wireless 1394.

Devices included in the definition of personal area networks (PANs) are those that are carried, worn, or located near the body. Specific examples include devices that are thought of as traditionally being networked, such as computers, personal digital assistants (PDAs), handheld personal computers (HPCs), and printers. Also included are devices such as digital imaging systems, microphones, speakers, headsets, bar-code readers, sensors, displays, and pagers, as well as cellular and personal communications service (PCS) phones.

The MBOA has been working for the past year with strong involvement from leading UWB companies, semiconductor manufacturers, and CE companies. This work has resulted in a new physical layer (PHY) and specifications based on UWB technology.

The technical requirements that form a basis for the standard are summarized in Table I. There are two modes of operation required, 110 and 200 Mb/s, with higher bit rates, such as 480 Mb/s, which are highly desirable. The desired range is 10 m for 110 Mb/s and can be reduced for higher bit rates. The system must be able to operate effectively in the presence of other systems sharing the same spectrum, such as IEEE 802.11a, as well as out-of-band systems such as IEEE 802.11b/g. It is also important that the power consumption be low to enable wireless connectivity for battery-operated portable devices.

The long-term vision for these products is to enable personal devices with integrated wireless connectivity. Market considerations require that products be implemented in CMOS in order to achieve low-power and low-cost integration with other devices [2]. This is the best ticket to fulfilling the vision of integrated connectivity.

II. UWB CHANNEL AND IEEE 802.15.3a STATISTICAL MODEL

All wireless systems must be able to deal with the challenges of operating over a multipath propagation channel, where objects in the environment can cause multiple reflections to arrive at the RX. For narrow-band systems, these reflections will not be resolvable by the RX when the narrow-band system bandwidth is less than the coherence bandwidth of the channel. As a result, narrow-band systems will experience multipath fading, or amplitude fluctuations, resulting from the constructive or destructive combining of the reflected paths. When there are a large number of arriving paths at the RX within its resolution time, the central limit theorem is commonly invoked in order to model the received envelope as a Rayleigh random variable. This Rayleigh fading channel model has been used extensively to model channels for cellular and many other wireless systems [3].

In contrast, the large bandwidth of UWB waveforms significantly increases the ability of the RX to resolve the different reflections in the channel. This characteristic of UWB systems has two main effects. First, the number of reflections arriving at the RX within the period of a very short impulse becomes smaller as the duration of the impulse gets shorter and shorter. As a result, the central limit theorem argument used to justify a Rayleigh distribution for the received signal envelope may not be valid. Therefore, the distribution of the received envelope caused by the channel multipath propagation required new measurements to understand. Second, as the multipath components may be resolved on a very fine time scale (proportional to the inverse of the signal bandwidth), the time of arrival of the multipath components may not be continuous. For example, multipath results from reflections off walls, ceilings, furniture, people, and other objects that may be present within a room. Since UWB waveforms can be up to 7.5-GHz wide, for example, paths separated by more than approximately 133 ps (equivalent to a 4-cm path length difference) can be individually resolved at the RX. Thus, different parts of the same furniture piece can give rise to several multipath components, all of which could be resolved by the RX. This phenomenon could partly explain the "clustering" of multipath components seen in the measurement, as described below (i.e., different objects or walls in a room could contribute different "clusters" of multipath components). Fig. 2 shows an example of an indoor channel measurement. This figure highlights a couple of the challenges the multipath model poses to UWB systems design. In particular, it shows that an indoor channel can have multipath components that extend over tens of nanoseconds. This will give rise to potential inter-symbol interference (ISI) when used for high-rate communications. In addition, it shows that a significant amount of energy exists in the multipath components. Therefore, RXs that can efficiently capture multipath components will benefit from greater received energy and extended range.

In order to get a better understanding of the indoor channel model, the IEEE 802.15.3a standards body asked for and received many contributions describing channel measurements and characteristics of those measurements (see [4][4] for a list of those contributions). These measurements showed several
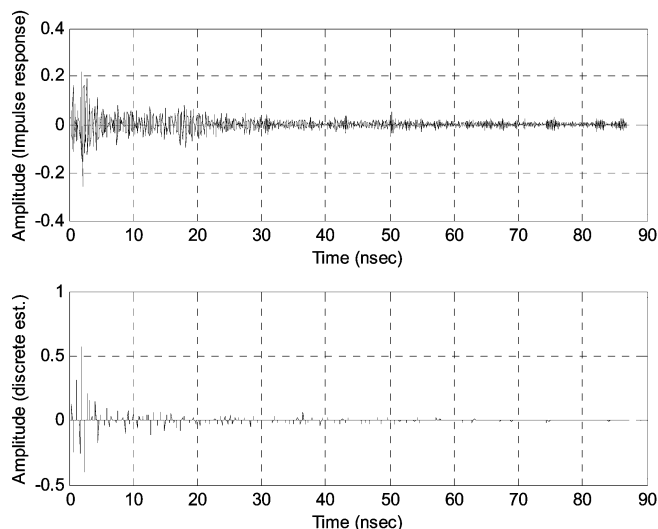
[4][Online]. Available: http://ieee802.org/15/

Fig. 2. Example channel realization from an indoor channel (the bottom figure is the discrete channel response with tap spacing of 167 ps, equivalent to the time resolution possible with a 6-GHz pulse).

unique characteristics for UWB channels, as discussed above. In particular, it was observed in many measurements that the multipath arrivals at the RX were not necessarily continuous in time. As a result, a multipath model, which captured the random arrival characteristics of the observed measurements seemed appropriate. Two previous indoor channel models that captured this type of channel behavior include the Saleh–Valenzuela (S–V) model [5] and the $\Delta - K$ model [6]. Both models use a statistical process to model the discrete arrivals of the multipath components, but the S–V model is unique in its approach of modeling arrivals in clusters, as well as rays within a cluster. This extra degree of freedom yielded better matching of the model to the channel characteristics gathered from measurement data. As a result, the IEEE 802.15.3a standards body selected the S–V model, which then needed to be properly parameterized in order to accurately reflect the unique characteristics of the measurements.

The SV model distinguishes between "cluster arrival rates" and "ray arrival rates," where the first cluster starts by definition at time $t = 0$, and the rays within the cluster arrive with a rate λ, given by a Poisson process with a start time relative to the cluster arrival time. It was observed in the measurements, as seen in Fig. 2, that the power of the multipath components decays over time. This was modeled as an exponentially decaying power profile with increasing delay from the first ray. The "cluster arrival rate," which is smaller than the ray arrival rate, determines when the next cluster begins.

Mathematically, the impulse response of the multipath model is described as

$$h_i(t) = X_i \sum_{l=0}^{L} \sum_{k=0}^{K} \alpha_{k,l}^i \delta\left(t - T_l^i - \tau_{k,l}^i\right)$$

where

- $\{\alpha_{k,l}^i\}$ are the multipath gain coefficients, i refers to the impulse response realization, l refers to the cluster, and k refers to the arrival within the cluster;

- $\{T_l^i\}$ is the delay of the lth cluster for the ith channel realization;
- $\{\tau_{k,l}^i\}$ is the delay of the kth multipath component relative to the lth cluster arrival time (T_l^i) (for the ith channel realization);
- $\{X_i\}$ represents the log-normal shadowing for the ith channel realization;
- Λ = cluster arrival rate;
- λ = ray arrival rate, i.e., the arrival rate of a path within each cluster.

By definition, $\tau_{0,l} = 0$. The distributions of the cluster arrival time and the ray arrival time are given by

$$p(T_l|T_{l-1}) = \Lambda \exp\left[-\Lambda(T_l - T_{l-1})\right], \qquad l > 0$$
$$p\left(\tau_{k,l}|\tau_{(k-1),l}\right) = \lambda \exp\left[-\lambda\left(\tau_{k,l} - \tau_{(k-1),l}\right)\right], \qquad k > 0.$$

The channel coefficients are defined as follows (the superscript i has been left off for simplicity):

$$\alpha_{k,l} = p_{k,l}\xi_l\beta_{k,l}.$$

In the above equations, ξ_l reflects the fading associated with the lth cluster, and $\beta_{k,l}$ corresponds to the fading associated with the kth ray of the lth cluster. As discussed previously, the small-scale fading statistics do not necessarily follow the Rayleigh distribution. After comparing different probability distributions to the measurement data, it was found that the log-normal distribution and the Nakagami distribution seemed to accurately reflect the measurement data. Due to its simplicity, the small-scale amplitude statistics were modeled as a log-normal distribution rather than the Rayleigh distribution, which was used in the original S–V model, which is reflected in the following equations:

$$20\log 10(\xi_l\beta_{k,l}) \propto \text{Normal}\left(\mu_{k,l}, \sigma_1^2 + \sigma_2^2\right)$$

or

$$|\xi_l\beta_{k,l}| = 10^{\frac{(\mu_{k,l}+n_1+n_2)}{20}}$$

where

$$n_1 \propto \text{Normal}\left(0, \sigma_1^2\right)$$

and

$$n_2 \propto \text{Normal}\left(0, \sigma_2^2\right)$$

are independent and correspond to the fading on each cluster and ray, respectively.

The behavior of the (averaged) power delay profile is

$$E\left[|\xi_l\beta_{k,l}|^2\right] = \Omega_0 e^{\frac{-T_l}{\Gamma}} e^{\frac{-\tau_{k,l}}{\gamma}}$$

which reflects the exponential decay of each cluster, as well as the decay of the total cluster power with delay. In the above equations, $p_{k,l}$ is equiprobable ± 1 to account for signal inversion due to reflections, and $\mu_{k,l}$ is given by

$$\mu_{k,l} = \frac{10\ln(\Omega_0) - \dfrac{10T_l}{\Gamma} - \dfrac{10\tau_{k,l}}{\gamma}}{\ln(10)} - \frac{\left(\sigma_1^2 + \sigma_2^2\right)\ln(10)}{20}.$$

Note that a complex tap model was not adopted here. The complex baseband model is a natural fit for narrow-band systems to capture channel behavior independently of carrier frequency, but this motivation breaks down for UWB systems where a real-valued simulation at RF may be more realistic.

Finally, the large-scale fading coefficient is also modeled as a log-normal random variable in order to capture shadowing effects in the channel (i.e., when objects block the line-of-sight component causing additional variation in the total average received energy). This effect is captured by the term X_i, where the total energy contained in the terms $\{\alpha_{k,l}^i\}$ is normalized to unity for each realization. This shadowing term is characterized by the following:

$$20\log 10(X_i) \propto \text{Normal}\left(0, \sigma_x^2\right).$$

In order to use the model, several of the above parameters need to be defined, which helps relate the model to actual measurements. Table II provides some target parameters for various line-of-sight and nonline-of-sight (NLOS) channels. The parameters of the model were found through an extensive search, which attempted to match the important characteristics of the statistical channel model output to the characteristics of actual measurements. The important channel characteristics included the mean excess delay, the rms delay spread, the mean number of paths within 10 dB of the peak (represented as $NP_{10\text{ dB}}$ in Table II), and the mean number of paths, which capture 85% of the channel energy. Note that the tabulated channel model parameters closely match the key characteristics of actual measurements. For example, when the bandwidth of the channel is very wide, the RX can resolve many paths that have useful energy. This characteristic of the channel impacts overall system design since it is apparent that a significant amount of energy exists in the multipath components. As will be seen in the remainder of this paper, orthogonal frequency-division multiplexing (OFDM) is an attractive modulation scheme for UWB communications because it can capture the multipath energy efficiently.

While the above model is quite general, it still contains a number of simplifications. First, it was assumed that the cluster and ray arrival rates are delay invariant. This is not necessarily the case, however, since reflected paths arriving at short separation distances are likely to be from the same object, while reflections seen at longer delays could come from a number of different objects within a room. This effect has also been shown in some measurements, but, in the interest of simplicity, the 802.15.3a model does not reflect that effect. Second, the model also assumes that the variance of the log-normal fading is independent of the delay. Again, this is not the most general case. An argument similar to the above shows that the relative variance should be smaller for small delays than for larger delays, a fact that was confirmed in [7]. Third, the channel model is based upon measurements only up to a 6-GHz bandwidth. As a result, it is unclear how well the model will match results in channels with a greater bandwidth, although similar trends and characteristics would be expected. Finally, the time variations (coherence time) of the channel were not considered here since most of the applications were based upon pedestrian speeds or slower. More

TABLE II
CHANNEL MODEL PARAMETERS AND COMPARISON WITH CHANNEL CHARACTERISTICS FROM MEASUREMENTS

Target Channel Characteristics[5]	CM 1[1]	CM 2[2]	CM 3[3]	CM 4[4]
Mean excess delay (nsec) (τ_m)	5.05	10.38	14.18	
RMS delay (nsec) (τ_{rms})	5.28	8.03	14.28	25
NP_{10dB}			35	
NP (85%)	24	36.1	61.54	
Model Parameters				
Λ (1/nsec)	0.0233	0.4	0.0667	0.0667
λ (1/nsec)	2.5	0.5	2.1	2.1
Γ	7.1	5.5	14.00	24.00
γ	4.3	6.7	7.9	12
σ_1 (dB)	3.3941	3.3941	3.3941	3.3941
σ_2 (dB)	3.3941	3.3941	3.3941	3.3941
σ_x (dB)	3	3	3	3
Model Characteristics[5]				
Mean excess delay (nsec) (τ_m)	5.0	9.9	15.9	30.1
RMS delay (nsec) (τ_{rms})	5	8	15	25
NP_{10dB}	12.5	15.3	24.9	41.2
NP (85%)	20.8	33.9	64.7	123.3
Channel energy mean (dB)	-0.4	-0.5	0.0	0.3
Channel energy std (dB)	2.9	3.1	3.1	2.7

[1] This model is based on LOS (0–4 m) channel measurements reported in [7].

[2] This model is based on NLOS (0–4 m) channel measurements reported in [7].

[3] This model is based on NLOS (4–10 m) channel measurements reported in [7], and NLOS measurements reported in [7].

[4] This model was generated to fit a 25-ns rms delay spread to represent an extreme NLOS multipath channel.

[5] These characteristics are based upon a 167-ps sampling time.

details of the model parameters and how to generate channel realizations can be found in [4], and readers interested in viewing some actual channel measurements can find them at a University of Southern California (USC) sponsored site.[5]

III. MODULATION OF CHOICE FOR UWB

The modulation of choice for UWB communications is application dependent and is driven by a number of parameters. For high data-rate UWB applications, performance, complexity, and system flexibility are the key criteria. The performance of the UWB system is determined by its robustness to multipath channel environments, ability to handle narrow-band interferers, and other UWB interferers. The ability to sculpt the transmit spectrum is also an important requirement as the UWB regulations have not been finalized in many countries.

Here, we motivate the suitability of OFDM by demonstrating that it satisfies the key criteria better when compared to a single-carrier approach. Although there are a number of modulation choices for UWB, for the sake of brevity, we restrict our attention to the multiband OFDM system and a single-carrier direct-sequence ultra-wideband (DS-UWB) approach based on M-ary bi-orthogonal keying (MBOK). In [9], the authors compare the computational complexity and multipath energy collection capabilities of the two remaining proposals in the IEEE

802.15.3a task group: a single-carrier DS-UWB system operating at a chip rate of 1368 MHz with a 16-finger RAKE; and a multicarrier UWB system with a 128-point fast Fourier transform (FFT), 60.6-ns cyclic prefix (CP), and an operating bandwidth of 528 MHz.

A. Performance in Multipath Channels

Multipath channel environments pose a significant design challenge for wireless communication systems. The performance and robustness of a wireless communication system is often determined by the amount of multipath energy that can be collected at the RX. As shown in Section II, the UWB channel models can be highly dispersive. For example, at distances between 4–10 m, the typical NLOS channel environment has an rms delay spread of 14 ns, while the worst case channel environment has an rms delay spread of 25 ns [4].

Depending on the type of system, there are typically two ways to collect multipath energy at the RX: either use a RAKE RX in a single-carrier system or insert a CP at the beginning of the transmitted symbol, as is often done in multicarrier systems, such as OFDM [8]. When the inverse of the sampling rate is significantly shorter than the total delay spread, as is the case for most UWB communication systems, OFDM systems become a more attractive system than a single-carrier system, especially in terms of complexity.

The performance of a single-carrier system in highly dispersive UWB channels is limited by two effects. Firstly, a large
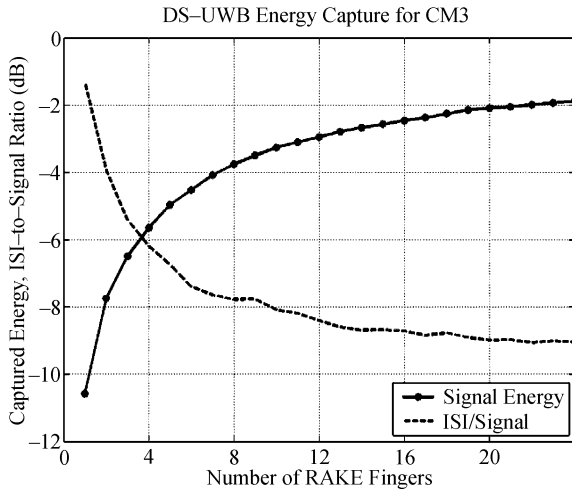
Fig. 3. 90th-percentile multipath energy capture of a DS-UWB system in 4–10-m NLOS channel environment.

number of RAKE fingers are needed in order to sufficiently capture multipath energy. Secondly, the time-dispersive nature of the channel causes ISI, resulting in performance degradation. The effect of ISI can be mitigated by the use of an equalizer, but this comes at the cost of added computational complexity.

Let the baseband equivalent discrete-sampled received sequence be represented as $r(n)$ with

$$r(n) = \sum_{k=0}^{L-1} h(k)s(n-k) + w(n)$$

where $s(n)$ is the transmitted sequence, $h(k)$ is the channel impulse response of length L, and $w(n)$ is the noise sequence. Let $y(n)$ represent the output of the RAKE RX with a span of L coefficients out of which only M fingers are nonzero. Let $\delta(k)$ represent the M delays corresponding to the nonzero coefficients of the L-tap RAKE RX response $f(n)$. Then

$$y(n) = \sum_{k=0}^{M-1} f\{\delta(k)\}r\{n-\delta(k)\}.$$

All the multipath energy can be captured if the RX filter response is matched to the channel impulse response. However, this implies that $M = L$, and would result in significant implementation complexity for the RAKE RX.

The loss in captured multipath energy and the signal-to-ISI ratio for the DS-UWB system is illustrated in Fig. 3 as a function of the number of RAKE fingers. The results are illustrated for the 90th-percentile channel realization corresponding to the 4–10-m NLOS channel environment (CM3) and a data rate of 114 Mb/s. It is assumed that the RAKE fingers are placed to capture the largest multipath coefficients within a span of approximately 40 μs. The plot shows that even with the optimal 16-finger RAKE, the DS-UWB system can only capture 56% of the available multipath energy. On the other hand, the multiband OFDM system, with a bandwidth of 528 MHz and a CP length of 60.6 ns, can capture approximately 95% of the multipath channel energy for the 90th-percentile channel realization in a CM3 channel environment.

With a 16-finger RAKE RX, the ISI term is only 9 dB below the signal energy and would consequently degrade system performance. Note that, as the data rate is doubled, the processing gain reduces by a factor of two and, consequently, increases the ISI term by 3 dB. For instance, the ISI value for a data rate of 200 Mb/s is approximately 5 dB below the signal energy for a 16-finger RAKE RX. Hence, without an equalizer, there is insufficient signal-to-interference and noise ratio (SINR) to successfully decode the information bits.

B. RX Complexity

The complexity of the RX is a critical parameter that determines the choice of the PHY. The complexity of the single-carrier system increases linearly with the number of RAKE fingers and the RX sampling rate. For the DS-UWB system, an M-finger RAKE RX requires M complex multiplies every chip. For a 16-finger RAKE RX implemented at chip rate sampling, 21.9 complex multiplies are required every nanosecond. Note that this complexity analysis for the DS-UWB system does not include the complexity required to implement a high-speed equalizer, which is often needed in single-carrier systems at high information data rates (>200 Mb/s).

The complexity of the OFDM system varies logarithmically with the FFT size. For an N-point FFT, $(N/2) \times \log_2(N)$ complex multiplies are required every OFDM symbol. Note that the OFDM symbol is typically longer than N samples due to the presence of a CP. For the multiband OFDM system the FFT requires 1.48 complex multiply operations every nanosecond.[6] The single-tap frequency-domain equalizer requires an additional 0.42 complex multiply operations every nanosecond resulting in a total RX complexity of 1.9 multiplies per nanosecond. Additionally, the multicarrier system needs no additional complexity to achieve the higher information data rates.

For highly dispersive channels, an OFDM RX is much more efficient at capturing multipath energy than an equivalent single-carrier system using the same total bandwidth. In addition to being able to efficiently capture energy, an OFDM system also possesses several other desirable properties, including high spectral efficiency, inherent resilience to narrow-band RF interference, and spectral flexibility, which is important because the regulatory rules for UWB devices have not been finalized throughout the entire world. The transmitted spectrum can easily be shaped by nulling out tones and/or turning off channels at the multiband OFDM TX in order to potentially protect sensitive or critical bands, e.g., radio astronomy bands.

IV. OVERVIEW OF MULTIBAND OFDM

Here, we will describe the multiband OFDM system and discuss the system design tradeoffs that must be considered when developing an OFDM-based system for the UWB spectrum. For the sake of simplicity, only a three-band multiband OFDM

---

[6]The FFT requires $64 \cdot \log_2(128)$ complex multiply operations every 160 samples and a sampling rate of 528 MHz.
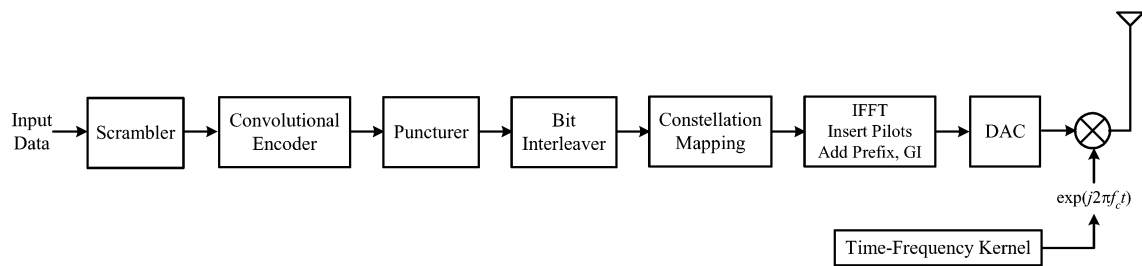
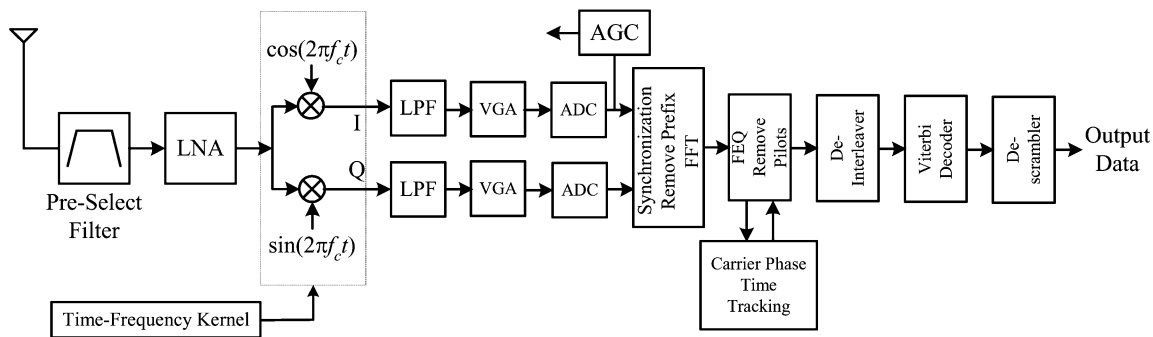Fig. 4.   Example TX architecture for a multiband OFDM system.

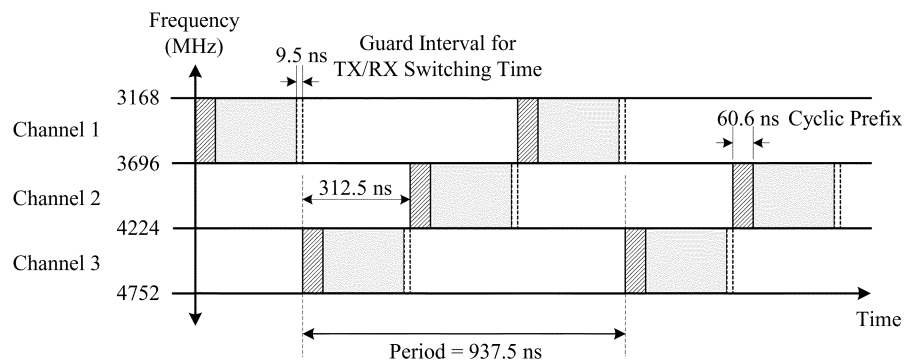Fig. 5.   Example RX architecture for a multiband OFDM system.

Fig. 6.   Example of time–frequency coding for the multiband OFDM system.

will be described herein. However, details about the full system, which has up to 14 sub-bands, can be found in [10] and [11].

A. Architecture for a Multiband OFDM System

One approach to designing a UWB system based on OFDM is to combine the modulation technique with a multibanding approach [12], which divides the spectrum into several sub-bands, whose bandwidth is approximately 500 MHz [10], [11]. The transmitted OFDM symbols are time-interleaved across the sub-bands. An advantage of this approach is that the average transmitted power is the same as a system designed to operate over the entire bandwidth. Other advantages of multibanding include processing the information over much smaller bandwidth (approximately 500 MHz), which reduces power consumption and lowers cost, improving spectral flexibility and worldwide compliance.

An example of a multiband OFDM TX and RX [10], [11] is shown in Figs. 4 and 5.

The TX and RX architectures for a multiband OFDM system are very similar to that of a conventional wireless OFDM

system. The main difference is that the multiband OFDM system uses a time–frequency kernel to specify the center frequency for the transmission of each OFDM symbol. An example of how the OFDM symbols are transmitted in a multiband OFDM is shown in Fig. 6.

Fig. 6 shows one realization of a time–frequency code, where the first OFDM symbol is transmitted on sub-band 1, the second OFDM symbol is transmitted on sub-band 3, the third OFDM symbol is transmitted on sub-band 2, the fourth OFDM symbol is transmitted on sub-band 1, and so on. For the sake of simplicity, this example shows a multiband OFDM system employing only three sub-bands and using a time–frequency code of length 3. In practice, the time–frequency code can be quite different and much longer in length. The time–frequency codes are used not only to provide frequency diversity in the system, but also to provide multiple access.

From Fig. 6, it is also apparent that a guard interval (9.5 ns) is appended to each OFDM symbol and that a CP is inserted before each OFDM symbol. The guard interval ensures that only a single RF transmit and RF RX chain are needed for all channel

environments and all data rates and that there is sufficient time for the TX and RX to switch between the different center frequencies.

B. Optimal Operating Bandwidth

An important parameter in the design of the multiband OFDM UWB system is the choice of the operating bandwidth. This choice impacts not only the link budget and, correspondingly, the overall system performance, but also affects the design of the TX and RX, especially the LNA, mixers, power consumption of the channel select filter, speed of the digital-to-analog converters (DACs), analog-to-digital converters (ADCs), and ultimately the speed at which the baseband needs to process the signal.

Two of the main parameters in the link budget table that are dependent on the operating bandwidth are the received signal power and noise figure. The received signal power is a function of the difference between the total transmit power and path loss. Since the FCC defines the average power in units of decibels referred to 1 mW per megahertz, the total transmitted power can be expressed completely in terms of the operating bandwidth. If the lower frequency f_L of the operating bandwidth is fixed at 3.1 GHz and upper frequency f_U is varied between 4.8–10.6 GHz, then the total transmit power $P_{TX}(f_U)$ can be expressed as follows:

$$P_{TX}(f_U) = -41.25 + 10\log_{10}(f_U - f_L) \text{ dBm.}$$

This equation assumes that the transmit PSD is flat over the entire bandwidth, which is an optimistic assumption, but sufficient for this analysis.

The path loss, which attenuates the transmitted signal, is also a function of the lower and upper frequencies of the operating bandwidth. The path-loss model specified by the IEEE 802.15.3a channel modeling committee is a free-space propagation model and is given as follows:

$$P_L(f_g, d) = 20\log_{10}\left[\frac{4\pi f_g d}{c}\right]$$

where f_g is the defined as the geometric average of the lower and upper frequencies, d is the distance measured in meters, and c is the speed of light.

In Fig. 7, the received signal power as a function of the upper frequency is plotted for a distance of 10 m. From this figure, it can be seen that the received power increases by, at most, 2.0 dB (3.0 dB) when the upper frequency is increased to 7.0 GHz (10.5 GHz). On the other hand, increasing the upper frequency to 7.0 GHz (10.5 GHz) results in the RX noise figure increasing by at least 1.0 dB (2.0 dB). Note that all relative changes in received power and noise figure were made with respect to an upper frequency of 4.8 GHz. Thus, the overall link margin will increase by, *at most*, 1.0 dB when increasing the upper frequency past 4.8 GHz; however, this comes at the expense of higher complexity and higher power consumption in current CMOS technology.

Another important criterion when selecting the operating bandwidth is that interferers may potentially lie within the bandwidth of interest. For example, in the U.S., the UNII
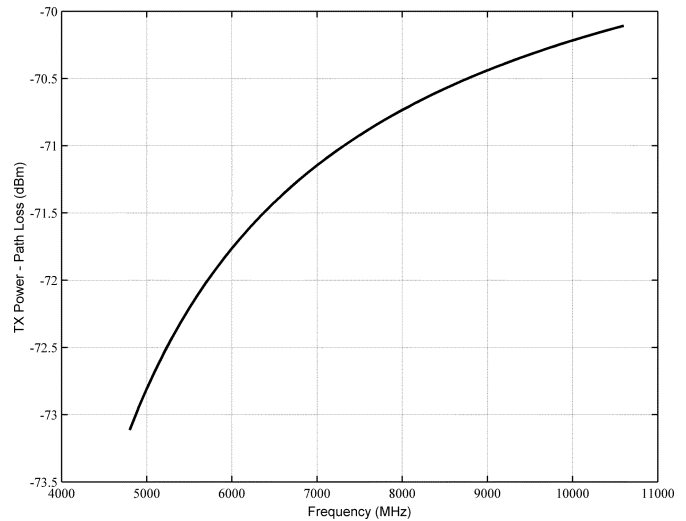

Fig. 7.   Received power as a function of upper frequency.

band occupies the bandwidth from 5.15 to 5.85 GHz; while in Japan, the UNII band occupies the bandwidth from 4.9 to 5.1 GHz. Both of these bands lie right in the middle of the UWB spectrum (see Fig. 1). By avoiding these bands (at least for initial devices), it is possible to simplify the design of the system, i.e., no complicated notch filters are required to suppress the interference.

Since the FCC specifies that a system must occupy a minimum of 500 MHz (10-dB) bandwidth in order to be classified as an UWB system, the maximum number of sub-band that can be placed between 3.1–4.8 GHz is only three. One possible option is to use a single sub-band that spans the entire operating bandwidth. However, the data rate requirements stated in Table I can be met by using a minimum bandwidth of 500 MHz. From an implementation point-of-view (lower power consumption for the channel select filter, lower speed for the ADCs, and lower speeds for the digital processing) and a multiple access point-of-view (larger selection of time–frequency codes), using a smaller sub-band bandwidth is much more desirable. Therefore, choosing a sub-band bandwidth as close to 500 MHz as possible is the optimal choice.

In the multiband OFDM UWB system, sub-band bandwidths of 528 MHz was chosen because it leads to a simple frequency plan and synthesize circuit (see Section IV-C) and it allows for sufficient transitions regions on either side of the three sub-bands for the design of the pre-select filter.

C. Frequency Planning and Synthesize Circuit

The frequency planning shown in Fig. 6 was chosen for two specific reasons. First, it allows sufficient guard band on the lower side of band 1 and the upper side of band 3 to simplify the design of a pre-select filter, which is used to attenuate the out-of-band signals (including emissions from the global positioning system (GPS), global system for mobile communications (GSM), PCS, industrial–scientific–medical (ISM) and UNII bands). Second, the particular center frequencies for the three-band system were chosen in such a way that it greatly simplifies the design of the synthesizer and ensures that system can
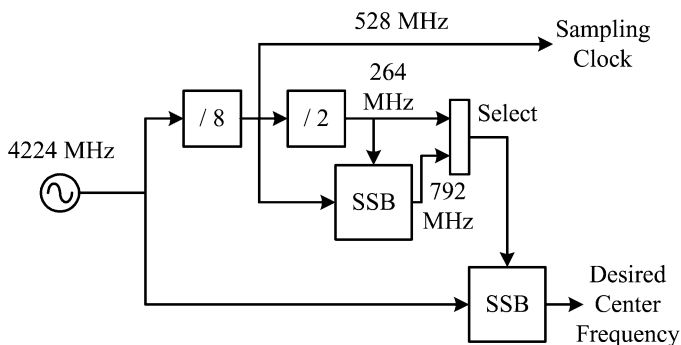
Fig. 8. Example synthesizer architecture that can switch between frequencies within a few nanoseconds.

switch between the center frequencies within a few nanoseconds.

An example of a block diagram for a synthesizer that can switch between three frequencies within a few nanoseconds is shown in Fig. 8. This synthesizer exploits the relationship between the center frequencies for the three-band system and oscillator. The basic idea is that each of the center frequencies is generated using a single-sideband beat product of the oscillator frequency with another frequency derived from the oscillator. The other frequency may be obtained from the oscillator frequency by using a combination of frequency dividers and single-sideband mixers. As an example, the center frequency for band 1 is generated by mixing 4224 MHz with 792 MHz to obtain a frequency of 3432 MHz. The 792-MHz signal is generated by mixing 528 MHz (= 4224/8) and 264 MHz (= 4224/16). The center frequencies for bands 2 and 3 can be obtained by mixing 4224 MHz with 264 MHz (= 4224 MHz/16).

The advantage of this architecture is that all of the center frequencies are generated from a single phase-locked loop (PLL). Since all of the center frequencies are available at all times, switching between the different sub-bands can be accomplished within a few nanoseconds. The exact time required for switching is limited by the response time of the multiplexer.

Fig. 9 depicts the plot from a circuit-level simulation of the frequency-switching architecture shown in Fig. 8. From this plot, it is clear that the nominal switching time is approximately 2 ns.

D. Optimal FFT Size

Another important parameter when designing an OFDM system is the size of the FFT. This block is typically 25% of the RX digital baseband complexity. Therefore, choosing an FFT size as small as possible is imperative. For the design of the multiband OFDM system, FFT sizes of 64 points ($\sim$51 kgates) and 128 points ($\sim$70 kgates) were considered. Since the multiband OFDM is targeted toward portable and handheld devices, an FFT size of 256 points ($\sim$91 kgates) is potentially too complex for low-cost low-complexity solutions. However, the use of a smaller FFT size increases the overhead due to CP and degrades the range.

The performance of the multiband OFDM system with a 64-point FFT and a prefix length of 41.7 ns, with a 64-point

FFT and a prefix length of 54.9 ns, and with a 128-point FFT and a prefix length of 60.6 ns was compared for the CM3 multipath channel environment specified in the IEEE 802.15.3a channel modeling sub-committee report [4]. A path-loss decay exponent of two was assumed for the simulations. All simulation results are averaged over at least 500 packets with a payload of 1 kB each. Note that the performance simulations incorporate losses due to front-end filtering, clipping at the DAC, ADC degradation (4 bits for 110/200 Mb/s and 5 bits for 480 Mb/s), multipath, shadowing, packet acquisition, channel estimation, clock frequency mismatch ($\pm$20 ppm at the TX and RX), carrier offset recovery, carrier tracking, etc.

The packet error rate (PER) performance in the CM3 channel environment is shown in Fig. 10 as a function of distance for an information data rate of 110 Mb/s. These plots correspond to the performance of the 90th best channel realization, i.e., the worst 10% channels are discarded. This implies that the performance of an actual multiband OFDM system will be better than what is illustrated in the plots for at least 90% of the channel realizations from each channel environment.

Fig. 10 shows that the 128-point FFT and a 60.6-ns prefix is approximately 0.9 dB better than the 64-point FFT and 54.9-ns prefix, and approximately 1.7 dB better than the 64-point FFT and 41.7-ns prefix. Thus, the optimal size for the FFT for the multiband OFDM system is 128 points, which provides an excellent balance between performance and complexity.

E. System Parameters

The system parameters for the multiband OFDM solution are given in Table III. This system is capable of transmitting data at information data rates of 55, 80, 110, 160, 200, 320, and 480 Mb/s. This system employs an OFDM scheme with a total of 128 sub-carriers. Out of the 128 sub-carriers, only 122 tones carry energy. Of the 122 sub-carriers, 100 are devoted to data, 12 are assigned to pilot tones, and the remaining ten are guard tones. In addition, the 122 sub-carriers are modulated using quadrature phase-shift keying (QPSK). By limiting the constellation size to QPSK, we can reduce the internal precision of the digital logic, specifically the inverse fast Fourier transform (IFFT) and FFT, and limit the precision of the ADCs and DACs. This helps to reduce the overall complexity of the system.

Forward error correction codes in conjunction with either frequency- or time-domain spreading are used to vary the information data rate of the system. The coding rates required by the different information data rates are generated by puncturing an industry standard $R = 1/3$, $K = 7$ convolutional code with generator polynomial $[133, 145, 175]_8$, where $[\cdot]_8$ refers to the octal representation of the polynomial. The exact puncturing patterns to generate the various coding rates are specified in [10] and [11]. The frequency-domain spreading is obtained by forcing the input data into the IFFT to be conjugate symmetric. The advantage of this type of spreading is that the output of the IFFT is always real; implying that only the real portion of the TX needs to be implemented.
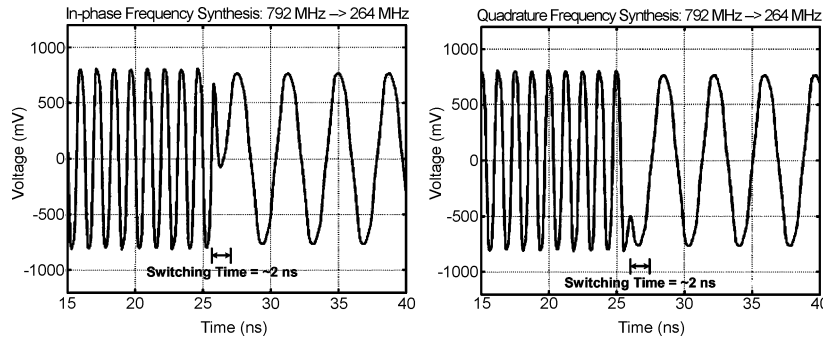
Fig. 9.   Circuit-level simulations of the frequency-switching architecture.
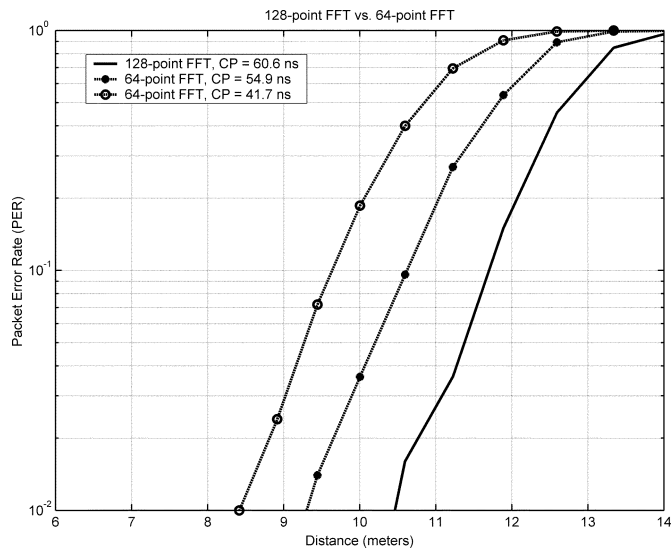

Fig. 10.   PER as a function of distance, and FFT size and prefix length for a data rate of 110 Mb/s.

F. Prefix Length

An OFDM system offers inherent robustness to multipath dispersion with a low-complexity RX. This property is a result of the addition of a CP. It can be shown that an RX using a CP forces the linear convolution with the channel impulse response to resemble a circular convolution [8]. A circular convolution in the time domain is equivalent to a multiplication operation in the discrete Fourier transform (DFT) domain. Hence, a single-tap frequency-domain equalizer is sufficient to undo the effect of the multipath channel on the transmitted signal.

The length of the CP determines the amount of multipath energy captured. Multipath energy not captured during the CP window results in inter-carrier-interference (ICI). Therefore, the CP length needs to be chosen to minimize the impact due to ICI and maximize the collected multipath energy, while keeping the overhead due to the CP small.

The UWB channel models are highly dispersive; a 4–10-m NLOS channel environment has an rms delay spread of 14 ns, while the worst case channel environment is expected to have an rms delay spread of 25 ns [4]. To illustrate the impact of CP length on system performance, the average captured energy for the 4–10-m NLOS channel environment, as well as the ICI introduced by the multipath energy outside the CP window, is depicted in Fig. 11. In this figure, the ICI-to-signal ratio is shown at

the input of the decoder and, hence, incorporates the processing gain that is expected for an information data rate of 110 Mb/s. To capture sufficient multipath energy and minimize the impact of ICI for all channel environments, the CP duration was chosen to be 60.6 ns [13].

Most conventional wireless OFDM-based systems use a CP to provide robustness against multipath. However, the same multipath robustness can be obtained by using a zero-padded (ZP) prefix instead of the CP [14]. The only modification that is required at the RX is to collect additional samples corresponding to the length of the prefix and to use an overlap-and-add method to obtain the circular convolution property.

The advantage of using a ZP prefix is that power backoff at the TX can be avoided. When a CP is used, redundancy or structure is introduced into the transmitted signal. This correlation in the transmitted signal leads to ripples in the average PSD. Since the UWB emissions are limited by the FCC, any ripples in the PSD will require power back off at the TX. In fact, the amount of power backoff that is required is equal to the peak-to-average ratio of the PSD. For a multiband OFDM system, this power backoff could be as large as 1.5 dB, which would result in a lower overall range for the system.

When a ZP prefix is used instead of the CP, the ripples in the PSD can be reduced to zero with enough averaging [14]. This is because the transmitted signal no longer has any structure; it is completely random. Fig. 12 illustrates the ripples in the PSD for a multiband OFDM system that uses a CP and ZP prefix. From this figure, it is clear that the ZP prefix will result in a PSD with zero ripples and, correspondingly, a zero power backoff at the TX, implying that the system will achieve the maximum range possible.

G. Link Budget Analysis for an Additive White Gaussian Noise (AWGN) Channel

Here, the link budget for a multiband OFDM system with data rates of 110, 200, and 480 Mb/s in an AWGN channel environment is examined. As required by the IEEE 802.15.3a selection criteria, we have assumed an isotropic antenna (0-dBi antenna gain) and path-loss exponent of two for the link budget calculations. In addition, the path-loss values are based on the geometric mean of the lower and upper frequency values. The geometric mean provides a more reasonable value for the expected path loss in the system.

TABLE III
MULTIBAND OFDM SYSTEM PARAMETERS

Info. Data Rate	55 Mb/s	80 Mb/s	110 Mb/s	160 Mb/s	200 Mb/s	320 Mb/s	480 Mb/s
Constellation	QPSK	QPSK	QPSK	QPSK	QPSK	QPSK	QPSK
FFT Size	128	128	128	128	128	128	128
Coding Rate (K=7)	R = 11/32	R = 1/2	R = 11/32	R = 1/2	R = 5/8	R = 1/2	R = 3/4
Frequency-domain Spreading	Yes	Yes	No	No	No	No	No
Time-domain Spreading	Yes	Yes	Yes	Yes	Yes	No	No
Data Tones	100	100	100	100	100	100	100
Prefix Length	60.6 ns	60.6 ns	60.6 ns	60.6 ns	60.6 ns	60.6 ns	60.6 ns
Guard Interval	9.5 ns	9.5 ns	9.5 ns	9.5 ns	9.5 ns	9.5 ns	9.5 ns
Symbol Length	312.5 ns	312.5 ns	312.5 ns	312.5 ns	312.5 ns	312.5 ns	312.5 ns
Channel Bit Rate	640 Mbps	640 Mbps	640 Mbps	640 Mbps	640 Mbps	640 Mbps	640 Mbps
Multi-path Tolerance	60.6 ns	60.6 ns	60.6 ns	60.6 ns	60.6 ns	60.6 ns	60.6 ns
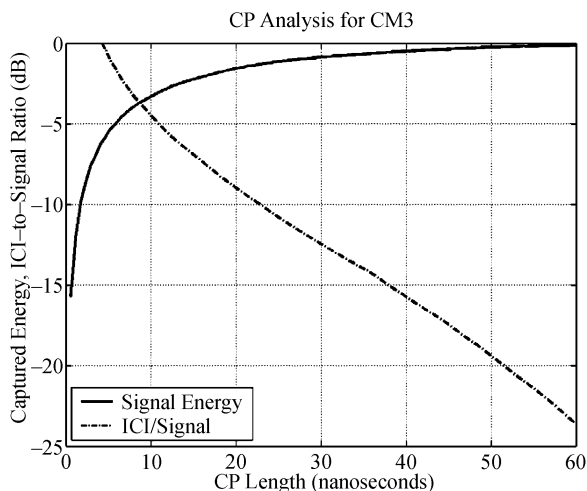
Fig. 11. Captured multipath energy as a function of CP length for a 4–10-m NLOS channel environment.

Fig. 12. PSD plots for an MB-OFDM system using: (a) a CP and (b) ZP prefix.

For the RX noise figure referred to the antenna terminal component of the link budget, the primary sources for the noise figure are the LNA and mixer. In this analysis, the circuit impedance is assumed to be 50 Ω. The voltage gain of the LNA is approximately 15 dB, while the voltage conversion gain of the mixer is approximately 10 dB. The total noise at the output of the LNA is 0.722×10^{-16} V^2/Hz. This value includes the noise of the LNA and the input of resistor. The total noise referred to the output of the LNA including the referred mixer noise is 0.722×10^{-16} V^2/Hz $+ 0.1 \cdot (8 \times 10^{-9})^2$ V^2/Hz$=$ 0.786×10^{-16} V^2/Hz, where the second term in the addition is generated by the noise sources within the mixer. Thus, the overall noise figure for the analog front-end is
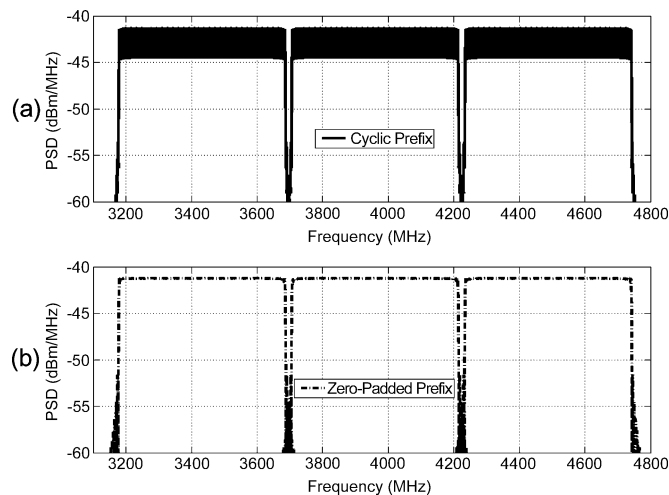
$10 \log_{10}(7.86/2.56) = 4.9$ dB. Including the losses associated with the pre-select filter (1.1 dB) and the transmit/receive switch (0.6 dB), the overall noise figure is 6.6 dB. Losses due to CP overhead, front-end filtering, clipping at the DAC, ADC degradation, channel estimation, clock frequency mismatch, carrier offset recovery, carrier tracking, etc. were included in the implementation loss component of the link budget. The implementation loss value used in the link budget was derived from the simulations results.

The link budget, presented in Table IV, shows that there is an excess link margin of 6 dB for a multiband OFDM system operating at an information data rate of 110 Mb/s at 10 m. For a device operating at 200 Mb/s at 4 m, there is an excess link margin of 10.7 dB. While for a device transmitting data at 480 Mb/s at

TABLE IV
LINK BUDGET ANALYSIS FOR AN AWGN CHANNEL

Parameter	Value	Value	Value
Information data rate (R_b)	110 Mb/s	200 Mb/s	480 Mb/s
Average Tx power (P_T)	−10.3 dBm	−10.3 dBm	−10.3dBm
Tx antenna gain (G_T)	0 dBi	0 dBi	0 dBi
$f_c' = \sqrt{f_{min} f_{max}}$: geometric center frequency of waveform (f_{min} and f_{max} are the -10 dB edges of the waveform spectrum)	3882 MHz	3882 MHz	3882 MHz
Path loss at 1 meter ($L_1 = 20 \log_{10}(4\pi f_c' / c)$) $c = 3 \times 10^8$ m/s	44.2 dB	44.2 dB	44.2 dB
Path loss at d m ($L_2 = 20 \log_{10}(d)$)	20 dB (d = 10 meters)	12 dB (d = 4 meters)	6 dB (d = 2 meters)
Rx antenna gain (G_R)	0 dBi	0 dBi	0 dBi
Rx power ($P_R = P_T + G_T + G_R - L_1 - L_2$ (dB))	−74.5 dBm	−66.5 dBm	−60.5 dBm
Average noise power per bit ($N = -174 + 10 * \log_{10}(R_b)$)	−93.6 dBm	−91.0 dBm	−87.2 dBm
Rx Noise Figure Referred to the Antenna Terminal (N_F)	6.6 dB	6.6 dB	6.6 dB
Average noise power per bit ($P_N = N + N_F$)	−87.0 dBm	−84.4 dBm	−80.6 dBm
Required E$_b$/N$_0$ (S)	4.0 dB	4.7 dB	4.9 dB
Implementation Loss (I)	2.5 dB	2.5 dB	2.5 dB
Link Margin ($M = P_R - P_N - S - I$)	6.0 dB	10.7 dB	12.7 dB
Proposed Min. Rx Sensitivity Level	−80.5 dBm	−77.2 dBm	−73.2 dBm

2 m, there is an excess link margin of 12.2 dB. The RX sensitivity for a system operating at 110, 200, and 480 Mb/s is −80.5, −77.2, and −73.2 dBm, respectively.

H. System Performance in Multipath Channel Environments

The performance of the multiband OFDM system is evaluated in both AWGN and multipath channel environments specified by the 802.15.3a channel modeling sub-committee report. A path-loss decay exponent of two was assumed for all the four channel environments. All simulations results are averaged over at least 500 packets with a payload of 1 kB each. Note that the performance simulations incorporate losses due to front-end filtering, clipping at the DAC, ADC degradation (4 bit for 110/200 Mb/s and 5 bit for 480 Mb/s), multipath, shadowing, packet acquisition, channel estimation, clock frequency mismatch (±20 ppm at the TX and RX), carrier offset recovery, carrier tracking, etc.

The PER performance in an AWGN channel is shown in Fig. 13 as a function of distance and the information data rate. The PER performance for the 90th-percentile channel realization is illustrated in Figs. 14–17 as a function of distance for the four-channel environments CM1–CM4, respectively. These plots correspond to the performance of the 90th best channel realization, i.e., the worst 10% channels are discarded. This implies that the performance of an actual multiband OFDM system will be better than what is illustrated in the plots for at least 90% of the channel realizations from each channel environment.
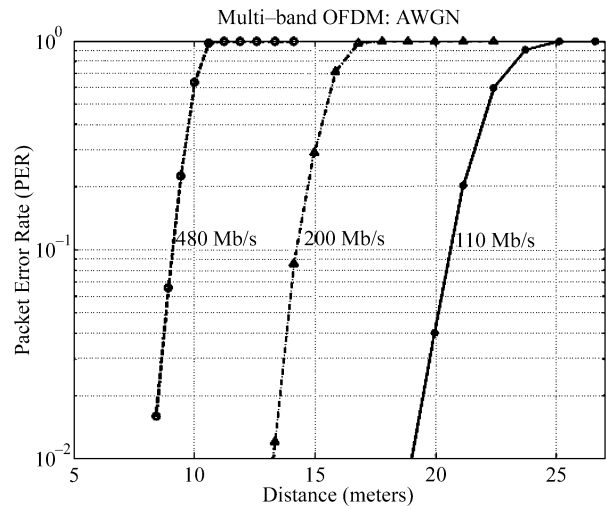

Fig. 13. PER as a function of distance and data rate in an AWGN environment.

Table V enumerates the achievable range that a multiband OFDM system can achieve in realistic multipath channel environments with a 90% link success probability. The link success probability is defined as the percentage of channel realizations for which the system can successfully acquire and demodulate a packet with a PER of less than 8%.

As the link success probability is dominated by shadowing and not by signal acquisition, the link success probability in an AWGN channel environment for the distance values listed in
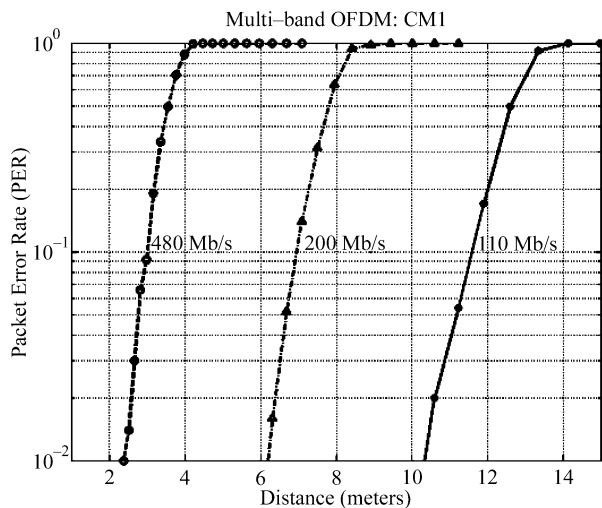
Fig. 14. PER as a function of distance and data rate in a CM1 channel environment for the 90th-percentile channel realization.
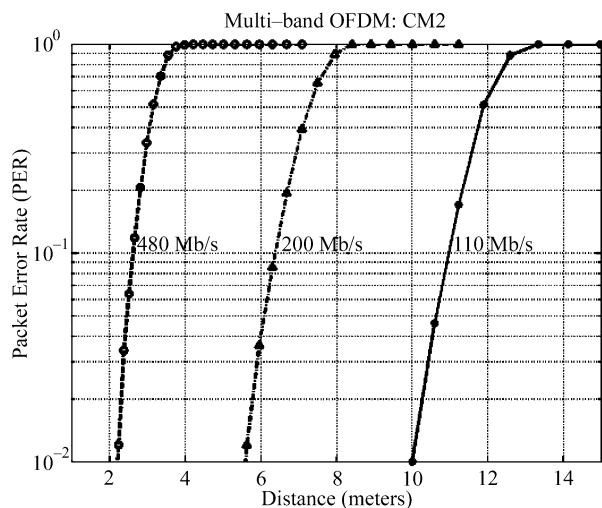

Fig. 16. PER as a function of distance and data rate in a CM3 channel environment for the 90th-percentile channel realization.

Fig. 15. PER as a function of distance and data rate in a CM2 channel environment for the 90th-percentile channel realization.

Fig. 17. PER as a function of distance and data rate in a CM4 channel environment for the 90th-percentile channel realization.

Table V is close to 100%. These results show that the multiband OFDM system can achieve a range of approximately 11 m in all multipath channel environments for an information data rate of 110 Mb/s. Furthermore, the multiband OFDM system can support data rates of 200 and 480 Mb/s at a distance of 5–6.9 and 2.6–2.9 m, respectively, in various multipath channel environments for a 90% link success probability.

As the multiband OFDM system has been designed to be robust to multipath and with a sufficiently long prefix, the performance is similar in the four channel environments. The small variations in performance are primarily due to the effect of shadowing that has been incorporated in the 100-channel realizations corresponding to each of the four-channel environments.

I. Multiple Access and Performance in Presence of Other Piconets

Another important design consideration for a UWB system is the performance of a UWB device in the presence of other UWB interferers. The performance is determined by the achievable
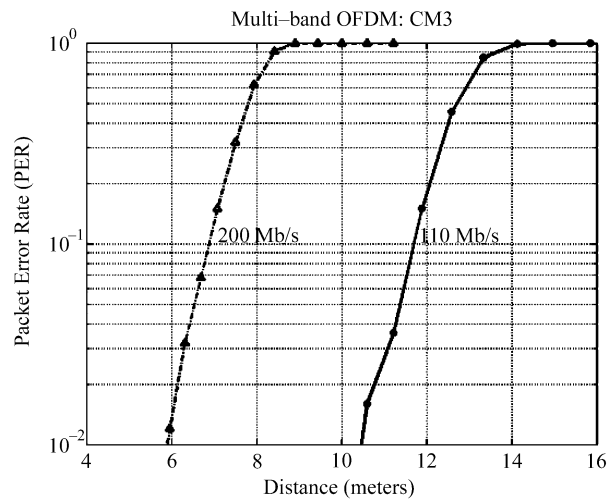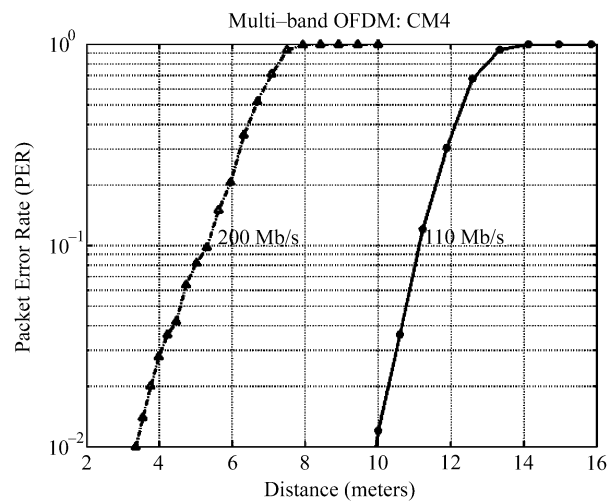
signal-to-interference ratio (SIR). In this case, the SIR is given as

$$\mathrm{SIR} = \left(\frac{P_{\mathrm{sig}}}{P_{\mathrm{int}}} \right) \left(\frac{W}{R} \right)$$

where P_{sig} is the power of the desired signal, P_{int} is the power of the interference, R is the information data rate, and W is the effective bandwidth of the transmitted signal. The first term in the above equation $(P_{\mathrm{sig}}/P_{\mathrm{int}})$ provides an indication of the distance separation between the UWB devices, whereas the second term in the above equation (W/R), which is denoted as bandwidth expansion factor, provides an indication of the processing gain available to suppress the interference. In the multiband OFDM system, the effective bandwidth is defined as follows:

$$W = \frac{N_B \times N_{DT}}{T_s}$$

where N_B is the number of bands, N_{DT} is the number of data tones, and T_s is the symbol duration.

From the above equations, it is clear that one way to improve performance in the presence of UWB interference is to ensure

TABLE V
RANGE AT WHICH THE PER FOR THE BEST 90% CHANNELS IS 8%

Data Rate	AWGN	CM1: LOS (0 – 4 m)	CM2: NLOS (0 – 4 m)	CM3: NLOS (4 – 10m)	CM4: Worst Case Delay Spread 25 ns
110 Mbps	20.5 m	11.4 m	10.7 m	11.5 m	10.9 m
200 Mbps	14.1 m	6.9 m	6.3 m	6.8 m	4.7 m
480 Mbps	8.9 m	2.9 m	2.6 m	—	—
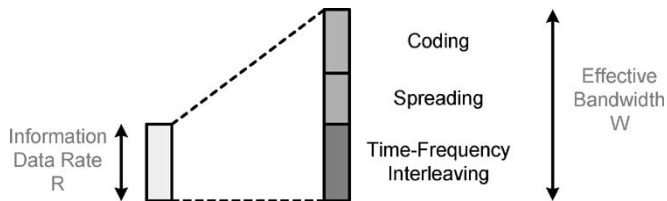
Fig. 18. Pictorial representation of bandwidth expansion.

TABLE VI
TIME–FREQUENCY CODES FOR DIFFERENT PICONETS

Piconet Number	Time Frequency Codes					
1	1	2	3	1	2	3
2	1	3	2	1	3	2
3	1	1	2	2	3	3
4	1	1	3	3	2	2

TABLE VII
PERFORMANCE IN THE PRESENCE OF UWB INTERFERERS AT A
DATA RATE OF 110 Mb/s

Channel Environment	1 Int. Device	2 Int. Devices	3 Int. Devices
CM1 (d_{int}/d_{ref})	0.40	1.18	1.45
CM2 (d_{int}/d_{ref})	0.40	1.24	1.47
CM3 (d_{int}/d_{ref})	0.40	1.21	1.46
CM4 (d_{int}/d_{ref})	0.40	1.53	1.85

that there is a sufficient separation between the reference devices and the interfering devices. Unfortunately, in practical applications it is impossible to constrain the distance between devices. The other approach is to try to make the bandwidth expansion factor as large as possible or, equivalently, the effective bandwidth as large as possible.

There are several ways to achieve bandwidth expansion. The two most common and well-understood techniques are time- and frequency-domain spreading and coding. In addition, the multiband OFDM system uses the previously mentioned two approaches and allows for a third and unique technique to be used to obtain bandwidth expansion: time–frequency interleaving. A pictorial representation of how the information data is expanded in bandwidth is shown in Fig. 18.

Essentially, time–frequency codes specify the center frequency for the transmission of each OFDM symbol.

As stated in Section I, the requirement for a UWB system is to support up to four piconets, which may potentially overlap. Since the spreading and coding techniques are independent of the piconet, the only way to achieve separation between the piconets (or equivalently devices) is to specify four unique time–frequency codes. One of the primary goals in the design of the time–frequency codes is to ensure that the average number of collisions between any two time–frequency codes is 1/3. The other goal is to ensure that the distribution of collisions should be as uniform as possible for all possible shifts of the codes. Using these two guidelines, four time–frequency codes, which are listed in Table VI, have been designed to have good collision properties for all possible asynchronous shifts among the piconets.

Given these four time–frequency codes, the performance of the multiband OFDM system was evaluated in the presence of other UWB interferers. The performance simulations incorporated losses due to front-end filtering, clipping at the DAC, ADC degradation (4 bits for 110 Mb/s), multipath, packet acquisition, channel estimation, clock frequency mismatch (± 20 ppm at the TX and RX), carrier offset recovery, carrier tracking, etc. In these simulations, the shadowing component was removed

from both the reference and interfering links by normalizing each channel realization to unit multipath energy. To evaluate the performance in the presence of interferers, the test link is established such that the reference link is set at a distance of $d_{ref} = 0.707$ of the 90% link success probability distance. The distance separation at which an interfering device can be tolerated is obtained by averaging the performance over all combinations of the reference link and interferer link channel realizations for each channel environment, where the reference and interferer link channel realization are specified in [4] and [16][7]. The d_{int}/d_{ref} values, where d_{int} is the distance between the reference RX device and the interfering device and d_{ref} is the reference distance between the reference TX and RX, are tabulated in Table VII as a function of the multipath channel environments and the number of interfering devices for an information data rate of 110 Mb/s.

These results show that a single interfering device can be brought within 3 m of the reference without causing any disruptions in the reference link. Naturally, as more interfering devices are added to the scenario, the separation distance between the reference RX device and interfering device must also be increased. These results were obtained by exploiting the time–frequency codes as well as the time-domain spreading techniques and using symbol erasures when collisions are detected. More details about the RX technique can be found in [17].

[7][Online]. Available: http://ieee802.org/15/

TABLE VIII
POWER CONSUMPTION NUMBERS FOR A MULTIBAND OFDM SYSTEM

Process Node	Rate (Mb/s)	Active Transmit Power	Active Receive Power	Clear Channel Assessment	Power Save (Deep Sleep Mode)
90 nm	110	93 mW	155 mW	94 mW	15 µW
	200	93 mW	169 mW	94 mW	15 µW
	480	145 mW	236 mW	94 mW	15 µW
130 nm	110	117 mW	205 mW	117 mW	18 µW
	200	117 mW	227 mW	117 mW	18 µW
	480	180 mW	323 mW	117 mW	18 µW

J. Complexity and Power Consumption

The total die size for the PHY solution is expected to be around 4.9 mm^2, with 3.0 mm^2 for the component area of the analog/RF portion and 1.9 mm^2 for the digital portion. These estimates assume a 90-nm CMOS technology node. If a 130-nm CMOS technology node is assumed, the total die size of the PHY solution is expected to be around 7.1 mm^2, with 3.3 mm^2 for the component area of the analog/RF portion and 3.8 mm^2 for the digital potion. The digital portion of the PHY is expected to require 295 kgates. The major external components that will be required by the complete solution (RF + PHY) are a pre-select filter, balun, crystal oscillator, and voltage regulator.

The multiband OFDM system is specifically designed to be a low-complexity CMOS-friendly solution. By limiting the constellation to QPSK, the resolution of the DAC and ADC converters, as well as the internal precision in the digital baseband, is lowered. The estimated power consumption of a multiband OFDM implementation as a function of data rate is enumerated in Table VIII. The power consumption calculations are provided for both a 90-nm CMOS technology node and a 130-nm CMOS technology node. In addition, for the 90/130-nm process node, a supply voltage of 1.5/1.8 V was assumed for the analog section of the PHY, except for the LNA where a 2-V supply was assumed. The digital section of the PHY requires a supply voltage of 1.2/1.3 V (for the 90/130-nm process node) and a clock of 132 MHz. Using these assumptions, the active power consumption for the transmit, receive, clear channel assessment (CCA), and power-save modes were calculated.

V. CONCLUSIONS

The FCC created a great opportunity in February 2002 when 7500 MHz of spectrum was allocated for unlicensed use of commercial UWB devices. The IEEE 802.15.3a task group has developed a channel model to estimate the performance of UWB systems in real-world environments. This has allowed designers to develop a specification, based on multiband OFDM, which meets the stringent market requirements: hundreds of megabits per second at low power and low cost. Several key organizations (MBOA, WiMedia, Wireless USB) have selected this design for their applications. OFDM already enjoys an outstanding record with other standards organizations, such as asymmetric digital subscriber line (ADSL), IEEE 802.11a, IEEE 802.11g, and IEEE 802.16a. In addition, OFDM was adopted for digital audio and terrestrial broadcast in both Europe and Japan. The choice by the UWB industry is based on the facts detailed in this paper that shows how multiband OFDM presents a very good technical solution for the diverse set of high-performance short-range applications that are eagerly anticipated by CE, PC, and mobile applications.

ACKNOWLEDGMENT

REFERENCES

[1] "First report and order, revision of part 15 of the commission's rules regarding ultra-wideband transmission systems," FCC, ET Docket 98-153, Feb. 14, 2002.

[2] D. Meacham and K. Soumyanath, "Standard CMOS ultrawideband single-chip solutions," *Elect. Eng. Times*, May 17, 2004.

[3] J. Proakis, *Digital Communications*, 4th ed. New York: McGraw-Hill, 2001.

[4] J. Foerster, Ed., "Channel modeling sub-committee report final,", IEEE802.15-02/490.

[5] A. Saleh and R. Valenzuela, "A statistical model for indoor multipath propagation," *IEEE J. Select. Areas Commun.*, vol. SAC-5, pp. 128–137, Feb. 1987.

[6] H. Hashemi, "Impulse response modeling of indoor radio propagation channels," *IEEE J. Select. Areas Commun.*, vol. 11, pp. 967–978, Sept. 1993.

[7] D. Cassioli, M. Z. Win, and A. F. Molisch, "The ultra-wide bandwidth indoor channel—From statistical model to simulations," *IEEE J. Select. Areas Commun.*, vol. 20, pp. 1247–1257, Aug. 2002.

[8] J. A. C. Bingham, "Multicarrier modulation for data transmission: An idea whose time has come," *IEEE Commun. Mag.*, vol. 28, pp. 5–14, May 1990.

[9] J. Balakrishnan, A. Dabak, S. Lingam, and A. Batra, "Complexity and performance analysis of a DS-CDMA UWB system,", IEEE P802.15-03/388r2, Sept. 2003.

[10] A. Batra *et al.*, "TI physical layer proposal for IEEE 802.15 task group 3a,", IEEE P802.15-03/142r2-TG3a, Mar. 2003.

[11] ——, "Multi-band OFDM physical layer proposal,", IEEE P802.15-03/268r0-TG3a, July 2003.

[12] V. S. Somayazulu, J. R. Foerster, and S. Roy, "Design challenges for very high data rate UWB systems," in *Proc. Asilomar on Systems, Signals, and Computation Conf.*, Nov. 2002, pp. 717–721.

[13] J. Balakrishnan, A. Batra, and A. Dabak, "A multi-band OFDM system for UWB communication," in *Proc. IEEE Ultra Wideband Systems and Technologies Conf.*, Reston, VA, Nov. 2003, pp. 354–358.

[14] B. Muquet, Z. Wang, G. B. Giannakis, M. de Courville, and P. Duhamel, "Cyclic prefix or zero padding for wireless multicarrier transmission?," *IEEE Trans. Commun.*, vol. 50, pp. 2136–2148, Dec. 2002.

[15] A. Batra, J. Balakrishnan, and A. Dabak, "Multi-band OFDM: A new approach for UWB," in *Proc. IEEE Int. Circuits and Systems Symp.*, vol. 5, Vancouver, BC, Canada, May 2004, pp. 365–368.

[16] R. Roberts, K. Siwiak, and J. Ellis, Eds., "P802.15.3a Alt PHY selection criteria,", IEEE P802.15-03/31r6-TG3a, Jan. 2003.

[17] S. Y. Park, G. Shor, and Y. S. Kim, "Interference resilient transmission scheme for multi-band OFDM system in UWB channels," in *Proc. IEEE Int. Circuits and Systems Symp.*, vol. 5, Vancouver, BC, Canada, May 2004, pp. 373–376.

Anuj Batra (M'00) received the B.S. degree (with distinction) in electrical engineering from Cornell University, Ithaca, NY, in 1992, the M.S. degree in electrical engineering from Stanford University, Stanford, CA, in 1993, and the Ph.D. degree in electrical engineering from the Georgia Institute of Technology, Atlanta, in 2000.

In 1992, he was with Raytheon E-Systems, Falls Church, VA, where he designed algorithms for a software-defined radio based on the Advanced Mobile Phone Service (AMPS) Standard. In 2000, he joined the Digital Signal Processing Solutions (DSPS) Research and Development Center, Texas Instruments Incorporated (TI), Dallas, TX. Since 2002, he has helped begin an internal UWB development effort within TI and co-developed the time–frequency interleaved OFDM (TFI-OFDM) proposal, which served as the foundation for the multiband OFDM proposal. This proposal defines a wireless UWB based PHY for high-speed communications (up to 480 Mb/s). In addition, he serves as the PHY Technical Chair for the MBOA, a partnership of over 140 of the companies in the CE, PC, home entertainment, semiconductor, and digital imaging segments. He is currently a Member, Group Technical Staff with TI. His research interests are in the areas of wireless communications, in particular, the design of high-speed wireless networks, multiuser detection theory, and coexistence between unlicensed wireless devices.

Dr. Batra is a member of Eta Kappa Nu and Tau Beta Pi. Since joining TI, he has also been involved in standardization activities for MBOA Special Interest Group (SIG), IEEE 802.15.3a, IEEE 802.11g, IEEE 802.15.2, and Bluetooth SIG.

Jaiganesh Balakrishnan (M'02) was born in Madras, India, in 1976. He received the B.Tech. degree in electrical engineering from the Indian Institute of Technology, Madras, India, in 1997, and the M.S. and Ph.D. degrees in electrical and computer engineering from Cornell University, Ithaca, NY, in 1999 and 2002.

Since 2002, he has been a Member of Technical Staff with the Digital Signal Processing Solutions (DSPS) Research and Development Center, Texas Instruments Incorporated, Dallas, TX. He co-developed the time–frequency interleaved OFDM (TFI-OFDM) UWB PHY proposal for high-speed wireless communications in PANs. The TFI-OFDM proposal served as the basis for the multiband OFDM proposal supported by the MBOA, a partnership of over 140 companies in the CE, PC, home entertainment, mobile phone, semiconductor, and digital imaging market segments. His research interests include detection and estimation, adaptive signal processing, and wireless communications, with specific emphasis on UWB and digital video broadcast.

Dr. Balakrishnan has been involved in standardization activities for IEEE 802.15.3a and the MBOA Special Interest Group (SIG).

G. Roberto Aiello (M'93) received the Ph.D. degree in physics from the University of Trieste, Trieste, Italy, in 1988.

He is founder and CEO of Staccato Communications Inc., San Diego, CA. He is a recognized leader in the UWB community and is actively involved in standards-setting committees. He was previously founder, President and CEO with Fantasma Networks (a UWB product company). Prior to being with Fantasma Networks, he was with Interval Research, in 1996, where he involved with advanced wireless technologies, and where he built the first documented UWB network. He previously held senior positions with the Stanford Linear Accelerator Center (SLAC), Menlo Park, CA, and the National Superconducting Super Collider Laboratory, Waxahachie, TX. He holds over 20 patents on UWB technology.

Dr. Aiello is a founding member of both the IEEE 802.15.3a and the 802.15.4a groups and of the MBOA. He has served and serves on several Advisory Boards such as iPASS and microwave photonics.

Jeffrey R. Foerster (M'98) received the B.S., M.S., and Ph.D. degrees from the University of California at San Diego, La Jolla, in 1994, 1996, and 1998, respectively. His doctoral thesis focused on adaptive interference suppression and coding techniques for code-division multiple-access (CDMA) systems.

In August 2000, he joined the Intel Laboratories, Intel Corporation, Hillsboro, OR, as a Wireless Researcher. He currently focuses on UWB and mobile broad-band wireless access technologies and co-manages a communications systems research group that is focused on advanced technologies for WPAN, wireless local area network (WLAN), and wireless metropolitan area network (WMAN) areas.

Anand Dabak (M'89) received the B.Tech. degree in electrical engineering from the Indian Institute of Technology, Bombay, India, in 1987, and the M.Sc. and Ph.D. degrees in electrical engineering from Rice University, Houston, TX, in 1989 and 1992, respectively.

He then joined Viasat Inc., Carlsbad, CA, where he was involved with satellite communications. In 1995, he joined Texas Instruments Incorporated, Dallas, TX, where he has since been involved with system and algorithm issues related to wireless communications. He is currently a Distinguished Member of Technical Staff and Manager of mobile wireless research with the Digital Signal Processing Solutions (DSPS) Research and Development Center, Texas Instruments Incorporated. He has been involved in the standardization activity in third-generation wireless systems, Bluetooth, and UWB systems. He holds 17 patents in the area of digital communications.